VISVESVARAYA TECHNOLOGICAL UNIVERSITY

BELAGAVI - 590018

PROJECT REPORT ON

"OPTIMIZATION OF PROGRAMME IN DRONE CONTROL SYSTEM USED FOR SEARCH OPERATIONS"

Submitted in partial fulfilment of the requirement for

BACHELOR OF ENGINEERING
IN
AERONAUTICAL ENGINEERING

SUBMITTED BY

AVESUDDIN SIDDIQUI	**1SJ17AE009**
MOHAN DC	**1SJ17AE027**
SATISH KUMAR H	**1SJ17AE039**
NANDAN KUMAR S	**1SJ17AE048**

Under the guidance of
Prof. VINAY P
Assistant Professor
Department of Aeronautical Engineering,
SJCIT, Chikkaballapura

Department of Aeronautical Engineering
SJC INSTITUTE OF TECHNOLOGY
CHICKBALLAPUR - 562 101

S J C INSTITUTE OF TECHNOLOGY

Department of Aeronautical Engineering

CERTIFICATE

This is to certify that the project work entitled **"OPTIMIZATION OF PROGRAMME IN DRONE CONTROL SYSTEM USED FOR SEARCH OPERATIONS"** carried out by **Mr. AVESUDDIN SIDDIQUI [1SJ17AE009], Mr. MOHAN DC [1SJ17AE027], Mr. SATISH KUMAR H [1SJ17AE039], Mr. NANDAN KUMAR S[1SJ17AE048],** are the bonafide students of S.J.C Institute of Technology in partial fulfillment for the award of the degree of **Bachelor of Engineering** in **Aeronautical Engineering** of the **Vishvesvaraya Technology University, Belgavi**during the year **2020 – 2021.** It is certified that all corrections/suggestions indicated for internal assessment have been incorporated and deposited to departmental library. The project report has been approved as it is satisfied academic requirements in respect of project work prescribed for the Bachelor of Engineering.

Vinay. P 13/8/21

Signature of the Guide **Signature of HOD** **Signature of Principal**

PROFESSOR & HEAD
Department of Aeronautical Engineering
S.J.C. Institute of Technology
Chickballapur - 562 101.

Principal
S.J.C. Institute of Technology
Chickballapur - 562 101.

EXTERNAL VIVA

NAME OF THE EXAMINERS	SIGNATURE WITH DATE
1)	
2)	

CHAPTER-1

INTRODUCTION

1.1. INTRODUCTION TO MAV

Micro Air Vehicle's (MAV) is small categories of an Unmanned Air Vehicle's (UAV) used for search and rescue operations. The size of a MAV starts from 5 cm. Usually MAV's operates at speed of 10-15m/s and with Reynolds number 10^4 -10^5.MAV's have relatively small sizes and weights compare to UAV's. Therefore, they are very suitable for military surveillance applications and image recording.

Figure 1.1: T-Hawk MAV

1.1.1. CLASSIFICATION OF MAV'S

a) Fixed wing configuration: Fixed wing models resemble to a conventional fixed wing aircraft. Fixed wing MAVs have high efficiency and long flight times. Fixed wing MAVs are usually preferred for long endurance and long range missions which require loiter and observation. Although they can fly faster compared to other configurations.

Figure 1.2: Typical fixed wing MAV

b) Rotary wing configuration: Rotary wing models have vertical take-off and landing capabilities and they can hover and move in any direction but with a limited flight time

compared to fixed wing configuration. In rotary wing configuration there are 3 different types,

i) Quad-rotor configuration: This configuration has four rotors. Two rotors (front and rear) rotate counter clockwise while other two (left and right) rotate in clockwise direction, so the torque created by the rotation of rotors are balanced. A quad-rotor system is controlled by changing the rotation of speed of rotors. It is mechanically simple but unstable and difficult to fly.

Figure 1.3 Pix-hawk Quad-rotor MAV

ii) Ducted fan MAV: It is composed of a type of propeller which is mounted on duct. The thrust is directed only to the back because the tip losses are reduced by the duct. Therefore, it is more efficient than a propeller. Ducted fan has the ability of thrust vectoring and produce lift just like fixed wing vehicle, so MAVs not only can hover but also can fly with forward speed.

Figure 1.4 iSTAR ducted fan MAV

iii) Co-axial rotors configuration: It has two rotors placed co-axially and rotating in opposite direction. There is no need for tail rotor, therefore all the available engine power is used for lift and thrust. The disadvantage is, the co-axial design requires a very complex hub mechanism.

Figure 1.5Skybotix CoaX Micro Helicopters

3) Flapping Wing Configuration: The interest in morphing wings stems from natural flight. Flapping wing MAVs are very light systems which imitate flights of birds and insects. They are not commonly used, but there are many studies on flapping wing configuration in order to make them compatible with the fixed wing and rotary wing MAVs.

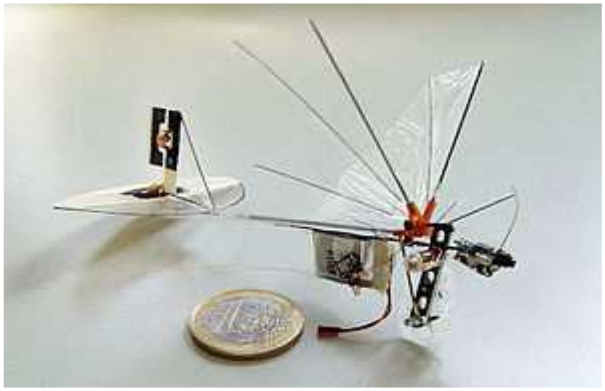

Figure 1.6:The DelFly Micro TU Delft

1.1.2. REYNOLDS NUMBER

The Reynolds number is the ratio of inertial forces to viscous forces and is a convenient parameter for predicting if a flow condition will be laminar or turbulent. It can be interpreted that when the viscous forces are dominant (slow flow, low Re) they are sufficient enough to keep all the fluid particles in line, then the flow is laminar. Even very low Re indicates viscous creeping motion, where inertia effects are negligible. When the inertial forces dominate over the viscous forces (when the fluid is flowing faster and Re is larger) then the flow is turbulent.

It is a dimensionless number comprised of the physical characteristics of the flow . An increasing Reynolds number indicates an increasing turbulence of flow.

It is given by,

$$\mathrm{Re} = \frac{\rho V D}{\mu}$$

Where, V = velocity of flow, m/s

D = chord length(diameter), m

ρ= density of fluid ,kg/m^3

μ = Dynamic viscosity, N s/m^2

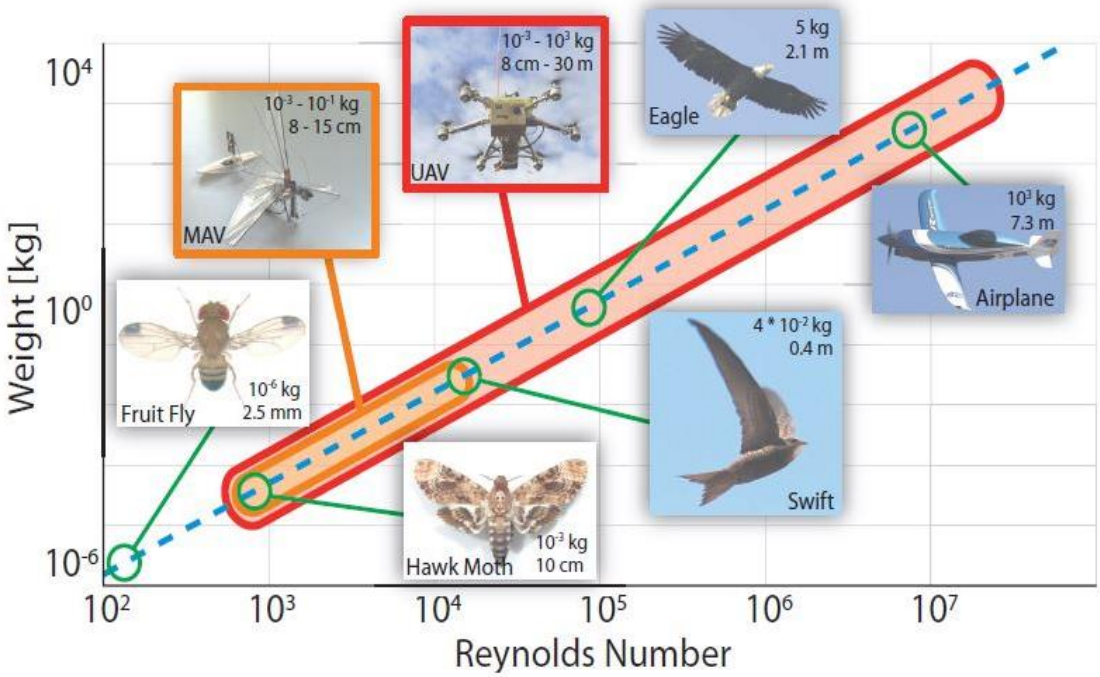

Figure 1.7: Comparison of unmanned aerial vehicles (UAV's,), micro air vehicles (MAV's)and other flyers.

1.2 INTRODUCTION TO BIO-INSPIRED AIRFOIL

1.2.1. Evolution of Bio-inspired aerofoil

Nature has presented us with everlasting mysteries which when seen in the dimension of engineering will give cognitive ideas for many high tech systems. A number of insects including locust, dragonfly, and damps fly employ wings that are not smooth or simple cambered surface. They are capable of being stationary in the same position in the air and to vary the flight direction instantly. This is because of the wing geometry and the musculature. The cross sections of the wings have well defined corrugations configuration.

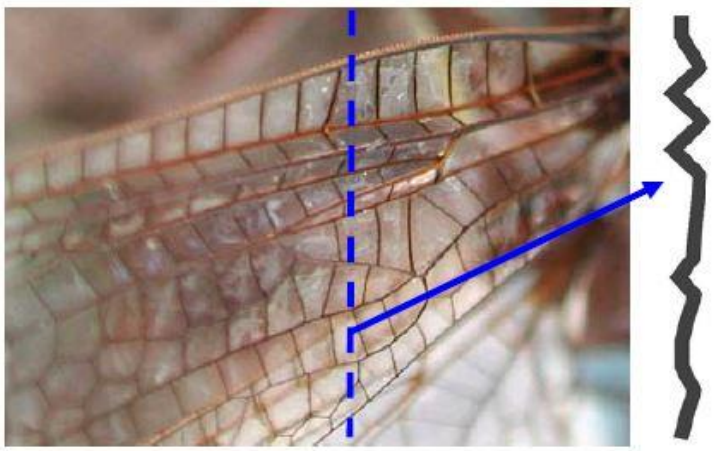

Figure 1.8: Dragon fly wing section

This corrugations are helped in stability of the ultra-light wings to handle the spanwise bending forces and mechanical wear that the wing experiances during flapping. Some of the research suggests that flow dynamics of a airfoils based on dragonfly wing cross-section. Bio-inspired airfoils with cross-sections resembling typical dragonfly wing cross-section and observed favoarable aerodynamic behaviour. They noted that flow separation vortices trapped within the corrugation valleys. These unique flow features mean that flow separations can be delayed in higher angle of attack with increasing in lift to drag ratio.

1.2.2. Advantage of Corrugated airfoil

- At low Reynolds number the influence of different geometrical parameters showed that the surface structure or roughness of wings results in an increased maximum lift co-efficient, C_{Lmax} and increase maximum lift to drag ratio.
- Dragonfly wings are highly corrugated, which increase the stiffness and strength of a Bio-inspired aerofoil during flapping.
- In Bio-inspired aerofoil due to corrugated structure the flow separation delays at higher angle of attack.

CHAPTER-2

LITRATURE SURVEY

2.1 Overview

Different tests are conducted for different conditions means they have come up with a simulation over a two corrugation aerofoils in a detailed design and a structural analysis with the help of catia, solid edge and they have tested an air flow over the aerofoil in ANSYS.

Then we are comparing a values executed by them and now we are comparing or testing it for a three corrugation aerofoil and getting the results.

Wei Hua Ho &T.H.New[1]

Here they conducted a computational fluid dynamics study on bio-inspired corrugated aerofoil at Reynolds number of 14000 by comparing a corrugated aerofoil with symmetrical NACA0010 aerofoil. In order to know aerodynamic performance of both the aerofoils. The method used was Ansys fluent 14.0, CFD .

In this the corrugated aerofoils suppress the flow separation under static flight conditions, by trapping the flow separation bubble within the corrugated valley. The separation bubble was smaller at AOA less than 15 degree.

The corrugated aerofoil also showed improved lift 5degree AOA. Drag was higher for the corrugated aerofoil which is intuitively expected. Dragonfly wing cross-section profiles tend to reduce the occurrence of flow separation events.

Varun Dhananjay Bhatt, Sanjay Mittal et.al[2]

This study was conduct the effect of corrugations on the aerodynamic performance of a Mueller C4 aerofoil, placed at a 5º angle of attack and Re = 10000. Here they used stabilized finite element method to solve the incompressible flow equations in 2d. This corrugation increases the aerodynamic performance compared to Mueller C4 aerofoil. Corrugation with more than one increases, the performance and 21% higher aerodynamic efficiency compared to C4 .Thus the shape led to higher lift and drag compared to c4 aerofoil. Downstream of the first corrugation, subsequent corrugations leads to decrement in drag.

T.H New, Shengxian Shi et.al [3]

This experiment was aimed at investigating the effects of corrugations on the flow separation control over an aerofoil. In this experimental set up on PIV over wind tunnel is used. The experiment was conducted in a low speed recirculating water tunnel with a test section. The test section was constructed from glass which allowed good optical access from the sides and bottom

Here visualizing two different corrugating aerofoils. Instead, their aerofoil has only two corrugations close to the leading edge (A), follows by a saddle and convex trailing edge hump (B). Corrugated B demonstrates better flow separation control behaviour and as a result, produces significantly smaller flow separation bubbles than corrugated A.

V.K.Sridhar, VEPA &Y.D Dwivedi[4]

Present study deals with the effect of bio-inspired corrugations variation of first peak shape is studied with triangular peak (model1) and a curved peak shape (model2) of aerofoil. Here the method they used ANSYS fluent software. The velocity and pressure contours for both the models are almost same. The lift forces of model 2 are little higher than model 1. The aerodynamic performance of a model 2 is found to be higher by 4.5% as compared to model 1.

P.Pradeep Kannah,G Balaji, S.Arunvinthan[5]

Here they conducted the project on "Aerodynamic characteristics of dragonfly wing sections". To study the local aerodynamic characteristics of different cross sectional sections of a dragonfly wing. In order to perform this project they used computational fluid dynamics. Dragonfly which has well defined cross-sectional corrugation can be interpreted as the ultra-light aerofoils during gliding.

The result is obtained from this project was highly remarkable optimizations in the shape of the aerofoil would result in positive spiral effect. This helps in reduction of wing area &aircraft structural weight.

Stefan Jongerius, D.Lentink[6]

This project aimed to determine the Structural analysis of a dragonfly wing by using Micro-CT Scanner method. To study how insect's wings carry aerodynamic and inertial loads, and how the resonant frequency of the flapping wings is tuned for carrying these loads. Based on computations they found that the inertial loads are 1.5 to 3 times higher than aerodynamic pressure loads.

The wings are highly corrugated which increases the stiffness and strength of the wing significantly and results in good aerodynamic performance .The vein and member thickness increases from tip to root , which allows the wing to effectively bear both inertial and aerodynamic load.

Maria Mingallon & Sakthivel Ramaswamy[7]

This paper studies the smart behaviour observed in the dragon fly wing combining advanced digital modelling techniques with non-linear structural analysis. This paper focused on several simulation studies of the forewing of Anisoptera. Structural analysis and CFD analysis were performed to understand the dynamics of a wing. Here they did further dynamic simulation of dragonfly wings such as Simulation of hind wing in combination with forewing, Simulation of the flow inside the veins, Highly flexible joints and the Anchorage points of the wing.

The cross sectional configuration varies greatly along the longitudinal axis of the wing rendering different local aerodynamic properties. The corrugations could aid is reducing wind drag & resistance in high rise constructions.

CHAPTER-3

3.1.OBJECTIVE

- To analyse the symmetrical and unsymmetrical aerofoil at low Reynolds number.
- To design and analyse the bio-inspired aerofoil with three corrugations at low Reynolds number.
- Evaluate the aerodynamic parameters.
- Comparison of all these three types of aerofoils at a given low Reynolds number.

CHAPTER-4

METHODOLOGY

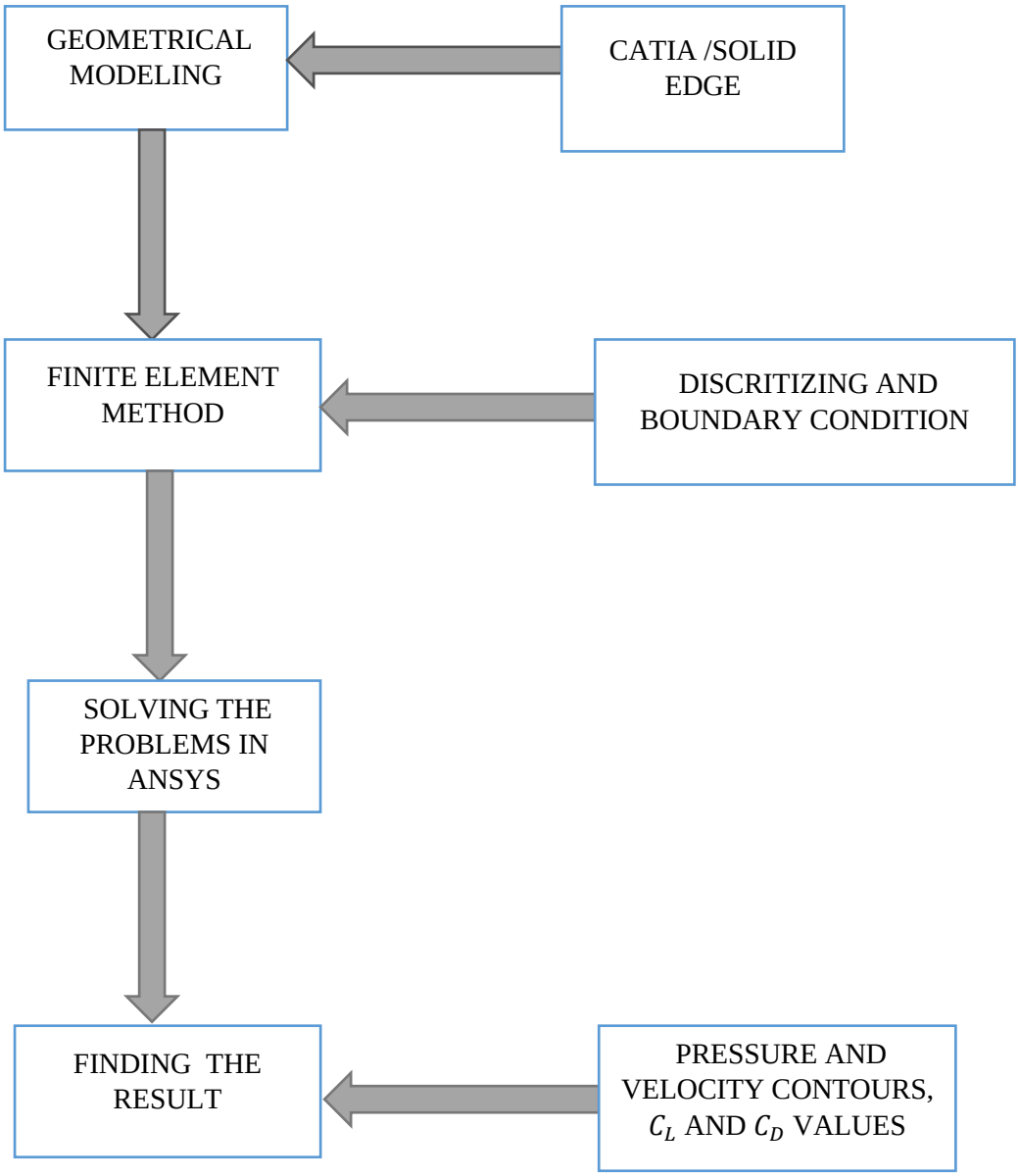

CHAPTER-5

5.1.PLAN OF EXECUTION

SL.NO	WORK	DATE
1	Collection of data from on-going projects, Searching for References, Introduction to project and literature survey	05-09-2019
2	Methodology	01-11-2019
3	Design of bio-inspired aerofoil using catia v5	15-12-2019
4	Analysis of Bio-inspired aerofoil	25-02-2020
5	Report writing and completion of project	01-03-2020

CHAPTER -6

COMPUTATIONAL ANALYSIS OF SYMMETRICAL AIRFOIL (NACA 0010)

6.1 Geometrical modelling of NACA 0010 air foil and domain

The air foil is symmetrical and it has maximum thickness at 10% of the chord.

The model is created using ANSYS. The coordinates for the model is provided in the appendix. After the coordinates are imported into ANSYS, the points are projected into 3D elements. And the point5s are connected to obtain the required air foil shape. The geometry is saved in the form of .igs format. The model is then imported to there meshing software, i.e., ICEM CFD where the far field boundary is created. Theoretically, the far field should be at least 10 times the chord length. Hence, the diameter of the far field is 1400mm, with its centre at the mid-point of the airfoil. The chord of the airfoil is 100mm.

Fig 6.1: NACA 0010 Airfoil

6.2 Discretization

O-grid type of mesh is created around the airfoil in ICEM CFD. It utilizes the method of blocking to create the mesh around the airfoil.

After the domain is specified around the airfoil, O-grid blocks are created in the far field, these blocks are associated with the far field and discretized into a greater number of elements by varying the number of nodes in the block. Similarly, the blocks near the airfoil are discretized into more elements, thus finer mesh is obtained near the airfoil.

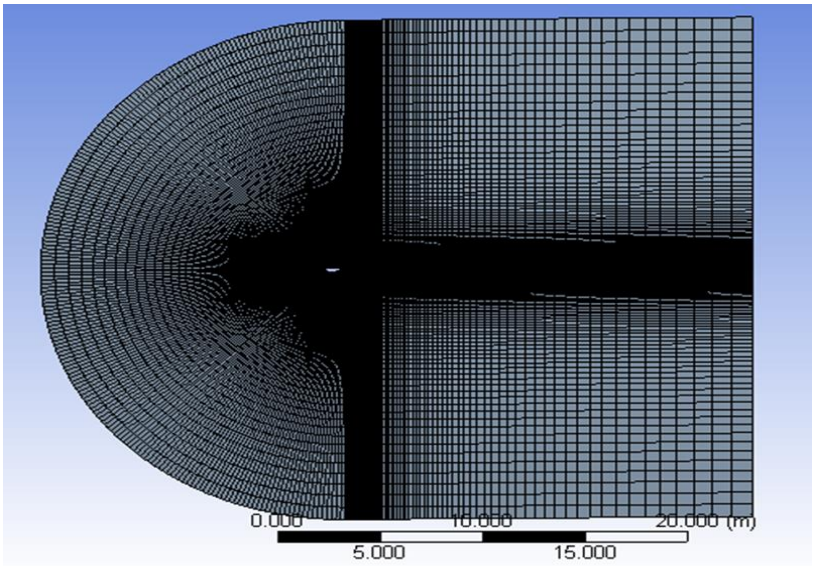

Fig 6.2: Mesh around NACA 0010 Airfoil

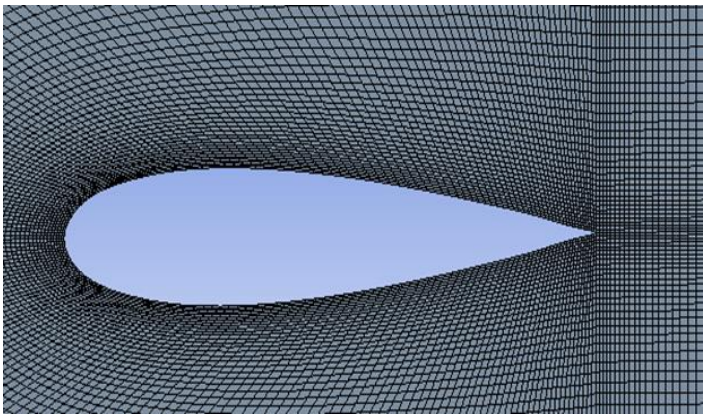

Fig 6.3: Mesh near NACA 0010 Airfoil

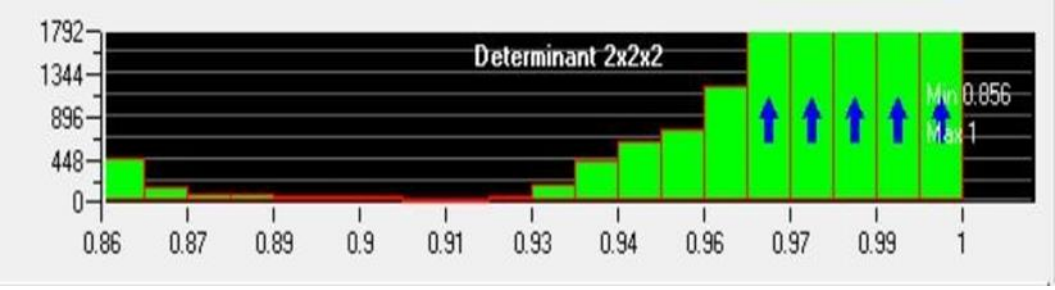

Fig 6.4: Mesh quality of NACA 0010 Airfoil

From fig 6.2, the element near the airfoil are represented by blue color and the elements in the far field are represented by pink color.

The mesh quality of NACA 0010 airfoil ranges from

The number of nodes and elements present in the mesh is given in the following table.

Table 6.1: Mesh information of the NACA 0010 Airfoil

Number of nodes	Number of elements
40535	40067

6.3 Boundary conditions

The boundary conditions to be initialized during the study are given in the Following table

Fig 6.2: Boundary conditions of NACA 0010 Airfoil

GENERAL a). solver b). time	 Pressure based Steady state
MODELS a). Energy equation b). Viscous	 On k-epsilon SST
FLUID	Air (Ideal gas)
BOUNDARY CONDITION a). Inlet b). Outlet c). Airfoil	 Velocity- inlet Velocity- 10m/s (in magnitude & direction) Pressure- outlet No slip condition
INITIALIZATION	Standard- Compute from inlet
PLOTS	C_l & C_d , Pressure & Velocity contours

The viscous model used here is the k-epsilon model which was specially developed for aerodynamic flows, and it is for low Reynolds number model.

Since the flow is to be studied at low Reynolds number model, the velocity is set as 10m/s approximately which is equal to 0.015M. This is also which the MAV's usually flies.

CHAPTER- 7

COMPUTATIONAL ANALYSIS OF CAMBERED AIRFOIL (NACA 2410)

7.1 Geometric modelling of NACA 2410 airfoil and Domain

NACA 4-digit series, NACA 2410, is chosen as the cambered airfoil. The first digit represents the maximum camber i.e., 2% of the chord length. The second digit represents the position of maximum camber i.e., 40% of the leading edge. The last two digits represent the thickness as the percentage of chord i.e., 10% of the chord.

The model is created using ANSYS. The coordinates for the model is provided in the appendix. After the coordinates are imported into ANSYS, the points are projected into 3D elements. And the points are connected to obtain the required airfoil shape. The geometry is saved in the form of .igs format. The model is then imported into the meshing software, i.e., ICEM CFD Where the far field boundary is created. Theoretically, the far field should be at least 10 times the chord length. Hence, the diameter of the far field is 1400mm, with its centre at the mid-point of the chord of the airfoil. The chord of the airfoil is 100mm.

Fig 7.1: NACA 2410 Airfoil

7.2 Discretization

O-grid type of mesh is created around the airfoil in ICEM CFD. It utilizes the method of blocking to create the mesh around the airfoil.

After the domain is specified around the airfoil, O-grid blocks are created in the far field, these blocks are associated with the far field and discretised into a greater number of elements by varying the number of nodes in the blocks. Similarly, the blocks near the airfoil are discretized into more elements, thus finer mesh is obtained near the airfoil.

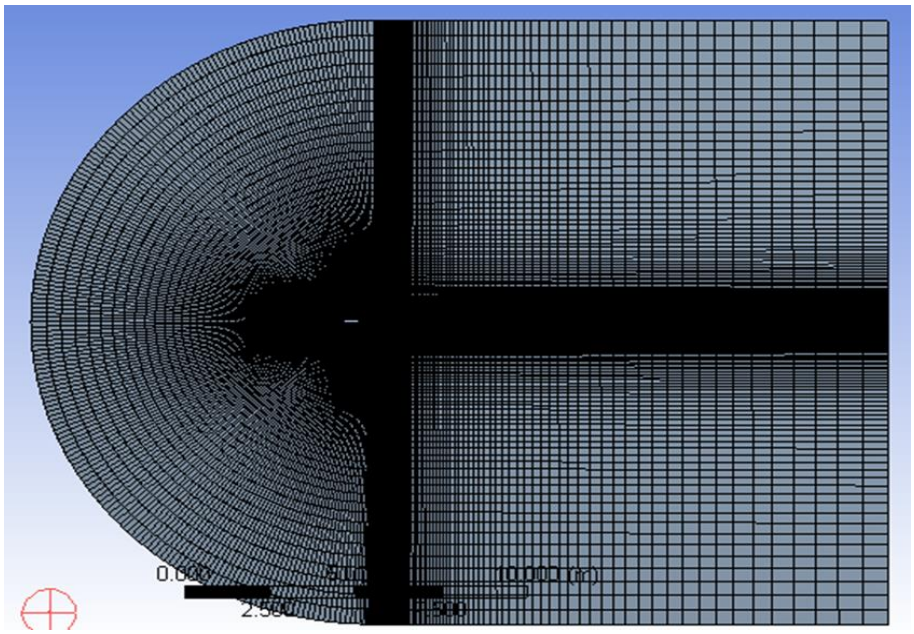

Fig 7.2: Mesh around NACA 2410 Airfoil

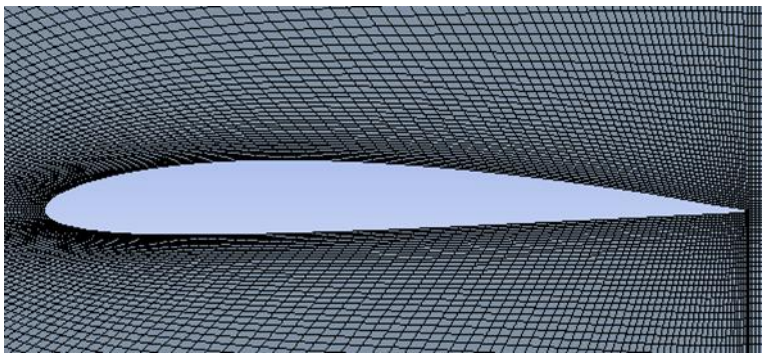

Fig 7.3: Mesh near NACA 2410 Airfoil

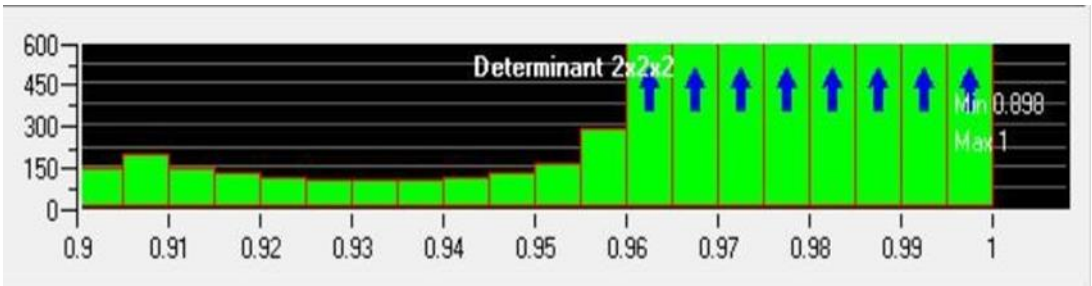

Fig 7.4: Mesh quality of NACA 2410 Airfoil

From Fig 7.2., the elements near the airfoil are represented by blue color and the elements in the far field are represented by pink color.

The mesh quality of the NACA 2410 airfoil ranges from 0.856 to 1. The number of nodes and elements present in the mesh is given in the following table

Table 7.1: Mesh information of NACA 2410 airfoil

Number of nodes	Number of elements
40746	40272

7.3 Boundary conditions

The boundary conditions to be initialized during the study are given in the following table

Fig 7.2: Boundary condition of NACA 2410 airfoil

GENERAL a). Solver b). Time	 Pressure based Steady state
MODELS a). Energy equation b). Viscous	 On k- epsilon SST
FLUID	Air (ideal gas)
BOUNDARY CONDITIONS a). Far field b). Outlet c). Airfoil	 Velocity- inlet Velocity- 10m/s (magnitude & direction) Pressure- outlet No slip condition
INITIALIZATION	Hybrid initialization
PLOTS	C_l & C_d , Pressure & Velocity Contours

The viscous model used here is the k-epsilon model which was specifically developed for aerodynamic flows and it is a low Reynolds number model.

Since the flow is to be studied at low Reynolds number, the velocity is set at 10m/s approximately which is equal to 0.010M. This is also the velocity at which the MAV usually flies.

CHAPTER- 8

COMPUTATIONAL ANALYSIS OF CORRUGATED AIRFOIL

8.1 Design of Corrugated Airfoil

The corrugated airfoil is mainly inspired by the wing structure of the dragonfly. The wing structure when viewed in normal to the place, it appears as a series of ridges. These ridges are commonly referred as corrugations.

Hence the current design of the corrugated airfoil model is limited to only two corrugations and has a curved streamlined trailing edge.

8.2 Geometric modelling of the corrugated airfoil

The model is created using ANSYS Fluent. The coordinates of the model is provided in the appendix. After the coordinates are imported into the ANSYS, the points shape. The geometry is saved in the form of .igs format. The model is then imported into the meshing software, i.e., ICEM CFD. Where the far field boundary is created. Theoretically, the far field should be at least 10 times the chord length. Hence, the diameter of the far field is 250mm, with its centre at the mid-point of the chord of the airfoil is 10mm.

Fig 8.1: Geometry of the corrugated airfoil

8.3 Discretization

O-grid type of mesh is created around the airfoil in ICEM CFD. It utilizes the method of blocking to create the mesh around the airfoil.

After the domain is specified around the airfoil, O-grid blocks are created in the far- field, there blocks are associated with the far field and discretized into a greater number of elements by varying the number of nodes in the block. Similarly, the blocks near the airfoil are discretized into more elements, thus finer mesh is obtained near the airfoil.

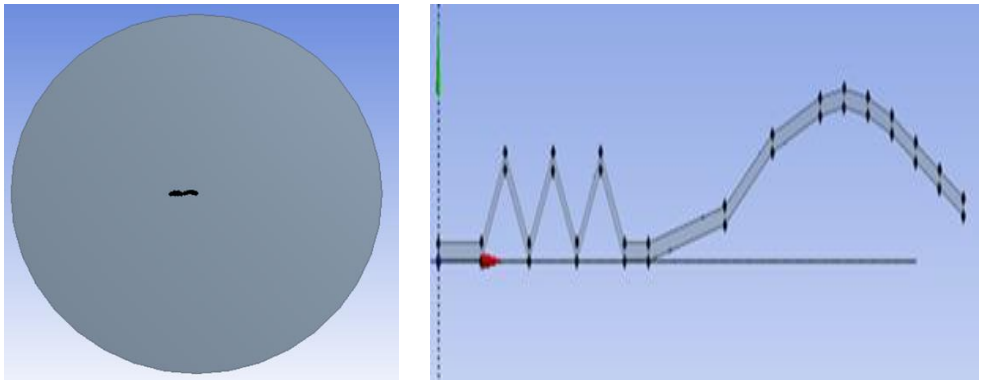

Fig 8.2: Corrigated airfoil with Far- Field boundary

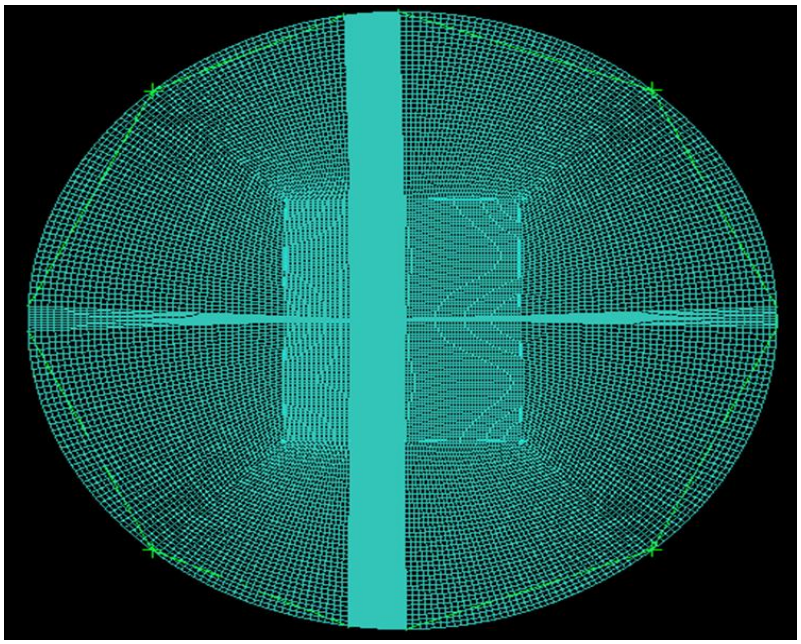

Fig 8.3: Mesh around the corrugated airfoil

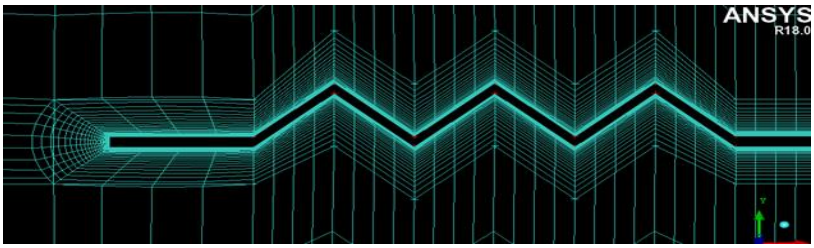

Fig 8.4: Mesh near the corrugations

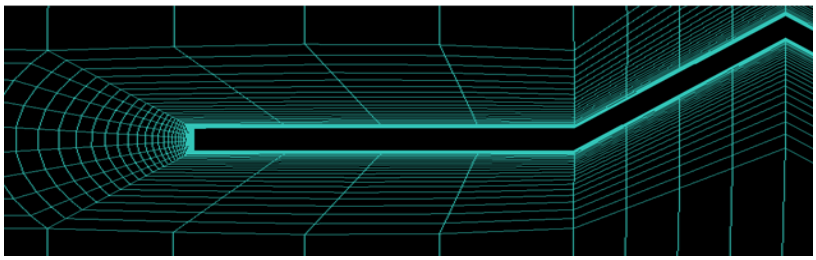

Fig 8.5: mesh near the boundary of the Corrugated airfoil

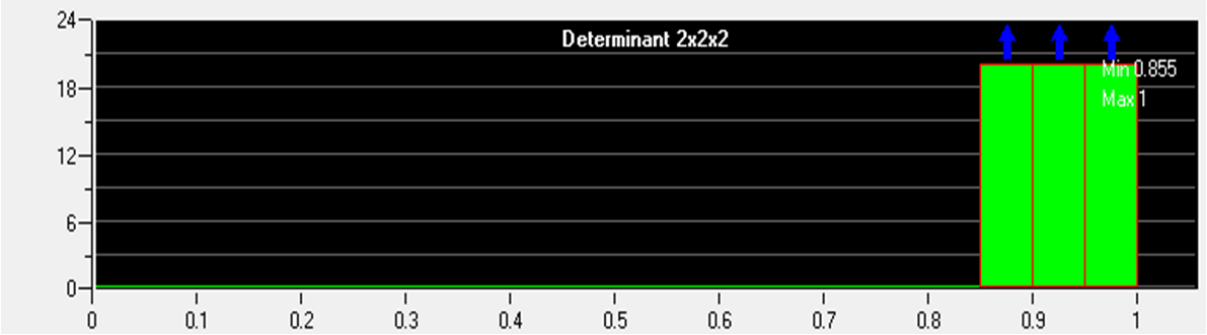

Fig 8.6: Mesh quality of the Corrugated airfoil

The mesh quality of the NACA 2410 airfoil ranges from 0.856 to 1. The number of nodes and elements present in the mesh is given in the following table.

Table 8.1: Mesh information of Corrugated airfoil

Number of nodes	36620
Number of elements	36290

8.4 Boundary Conditions

The boundary conditions to be initialized are given in the following table

Table 8.2: Boundary conditions for Corrugated airfoil

GENERAL a). Solver b). Time	 Pressure based Steady state
MODELS a). Energy equation b). Viscous	 On k-epsilon SST
FLUID	Air (ideal gas)
BOUNDARY CONDITIONS a). Far- Field b). Outlet c). Airfoil	 Velocity- inlet Velocity- 10m/s(magnitude & direction) Pressure- outlet No slip condition
INITIALIZATION	Standard- Compute from inlet
PLOTS	C_l & C_d , Pressure & Velocity Contours

The viscous model used in this study is k-epsilon SST model. Although the flow is said to be laminar, as it passes over the corrugations the flow will slightly turn turbulent due to the formation of eddy currents which get trapped in the ridges.

CHAPTER- 9

RESULTS AND DISCUSSIONS

9.1 Results of NACA 0010 Airfoil

After the boundary conditions specified for the airfoil is initialized and the calculation are completed the following CFD results are available.

Table 9.1: CFD results of NACA 0010 airfoil at velocity of 10m/s

AOA	C*l*	C*d*	C*l* /C*d*
0	0	0.01971	0
5	0.05865	0.02741	2.139
7	0.07375	0.04575	1.612
10	0.05869	0.12479	0.470
12	0.06479	0.15831	0.409
15	0.07007	0.19972	0.351

17	0.07584	0.23233	0.326
20	0.08316	0.2662	0.312

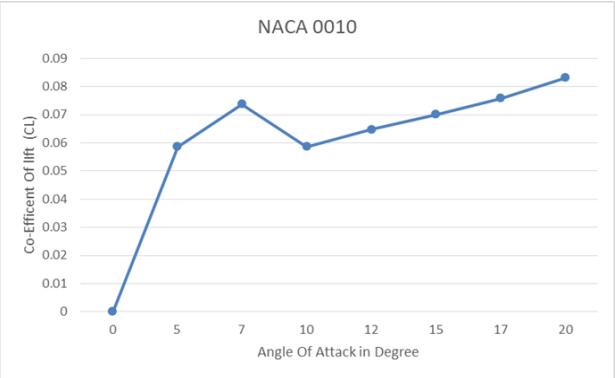

Fig 9.1: C*l* vs AoA of NACA 0010 Airfoil

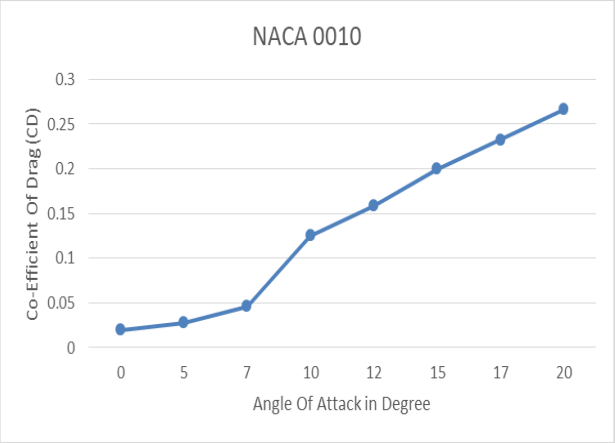

Fig 9.2: C*d* vs AoA of NACA 0010 Airfoil

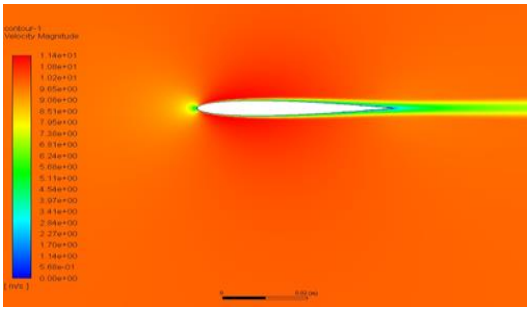

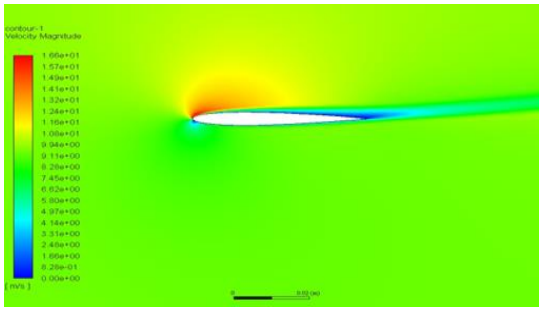

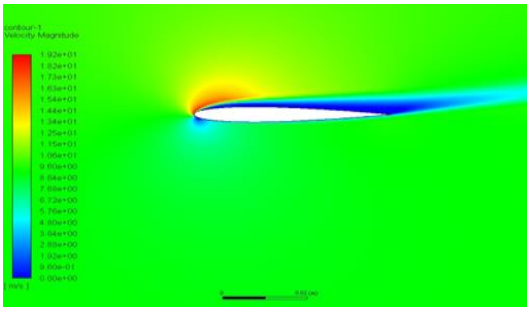

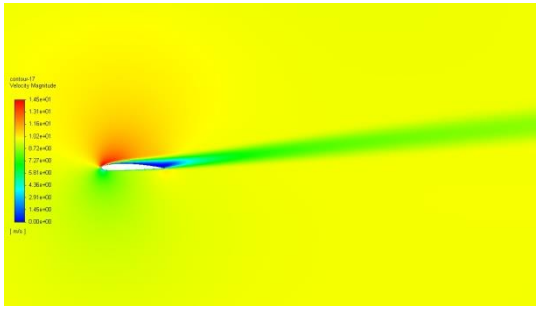

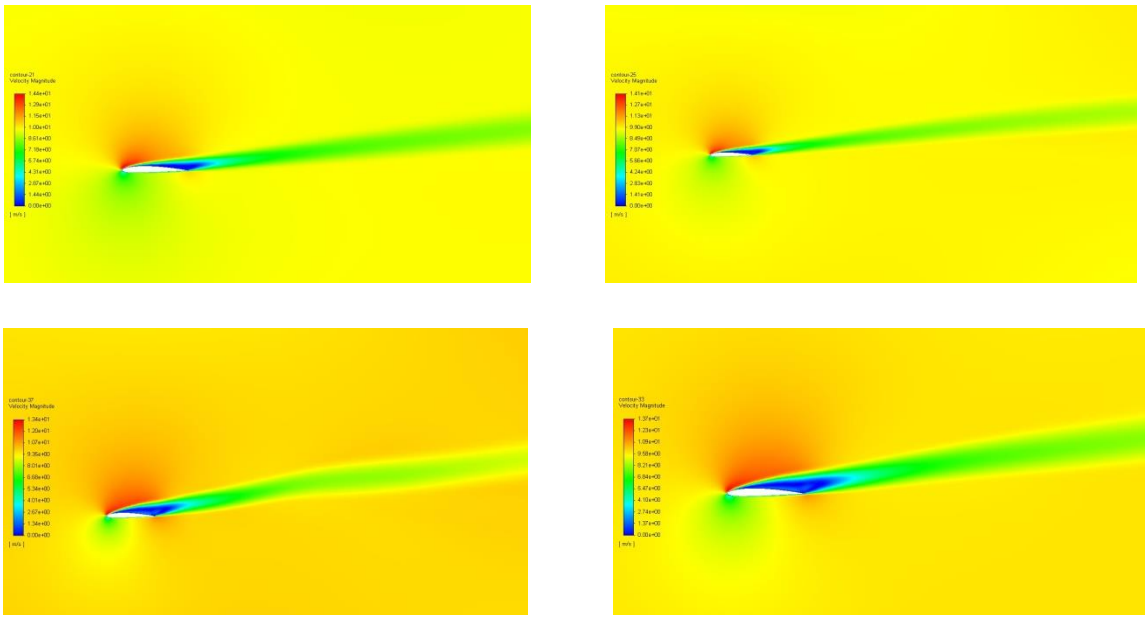

Fig 9.3: Velocity contours of NACA 0010 Airfoil at 0° (top left), 5° (top right), 7° (second left), 10° (second right), 12° (third left), 15° (third right), at stalling angle 17° (bottom left), and 20° (bottom right)

From Fig 9.1 which shows a graph between the co-efficient of lift and angle of attack and Fig 9.2 which shows a graph between the co-efficient of drag and angle of attack, we can deduce that the co-efficient of lift and drag for NACA 0010 airfoil linearly varies with increasing angle of attack. Stall condition occurs at 15° where further increase in the angle of attack results in decrease in the co-efficient of lift and drag due to the flow being separated from the boundary or surface of the airfoil.

From Fig 9.3 of velocity contours, it can be seen that the airfoil has equal velocity near bopth the upper and lower surface of the airfoil,. The velocity above and below he airfoil is equal to the free stream velocity above the biundary layer of the airfoil. The velocity at the leading edge and trailing edge areslightly less when compared to the fres stream velocity. The airfoil gets obstructed by the leading surface of the airfoil, thus creating a stagnant point near the leading edge. As the angle of attack increases, the stagnant point starts moving towards the trailing edge. The flow over the uppervsurface of the airfoil gets separated from the boundary.

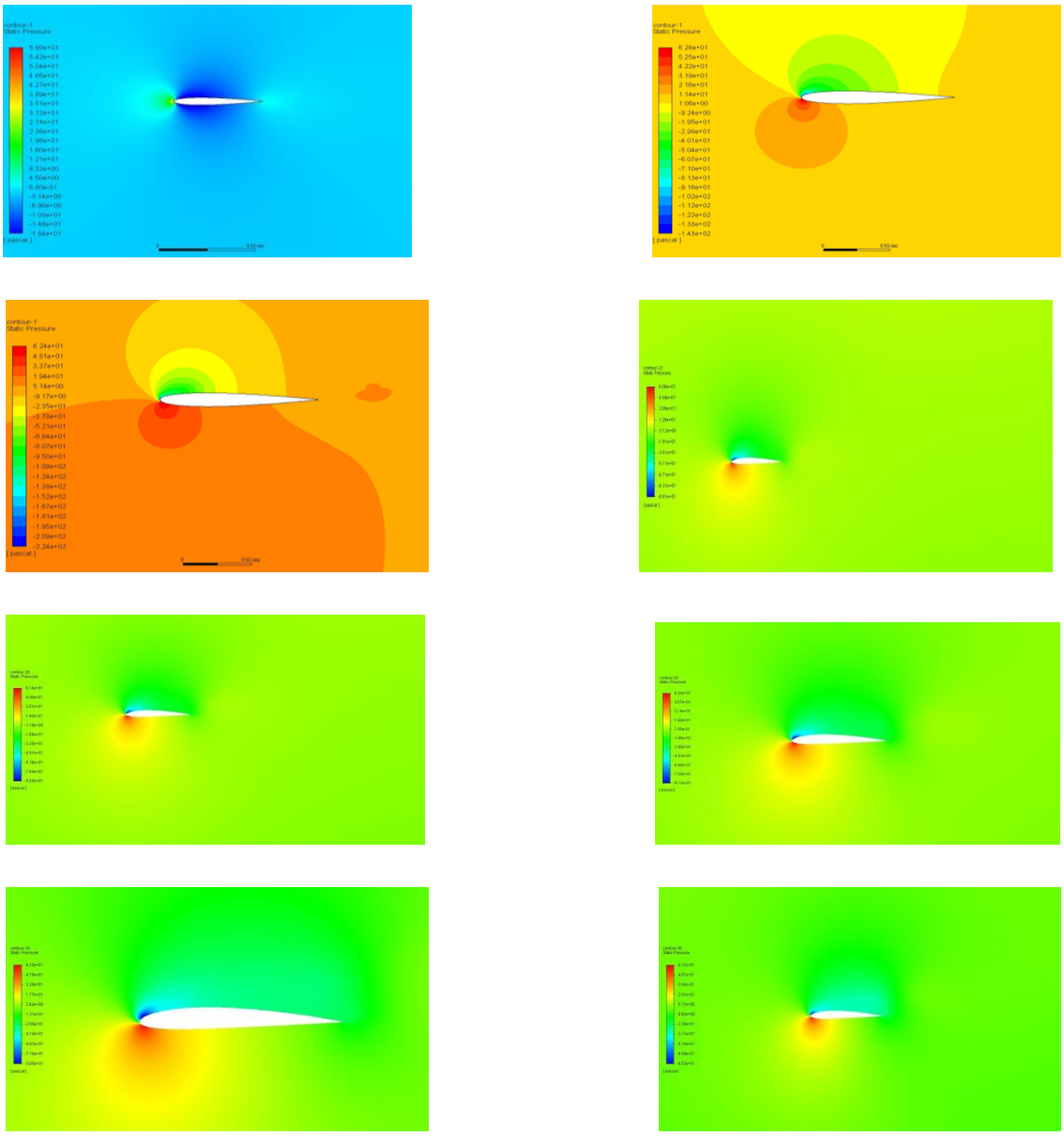

Fig 9.4: Pressure contours of NACA 0010 airfoil at 0° (top left), 5° (top right), 7°(second left), 10° (second right), 12°(third left), 15°(third right), at stalling angle 17°(bottom left), 20°(bottom right)

From Fig 9.4, of pressure contours it can be seen that upper surface having lower pressure and lower surface has higher pressure. This situation shows that pressure on lower side tries to lift the body and hence increases the lift co-efficient. In the given figure of pressure contours it is shown that at the leading edge of the upper side there is a greenish colour and on the lower side the colour is reddish, where red colour indicates a higher value of pressure and greenish colour indicates a lower value. As the angle of attack increases, the coefficient of lift also increases but after 17°-20° of angle of attack, it starts decreasing.

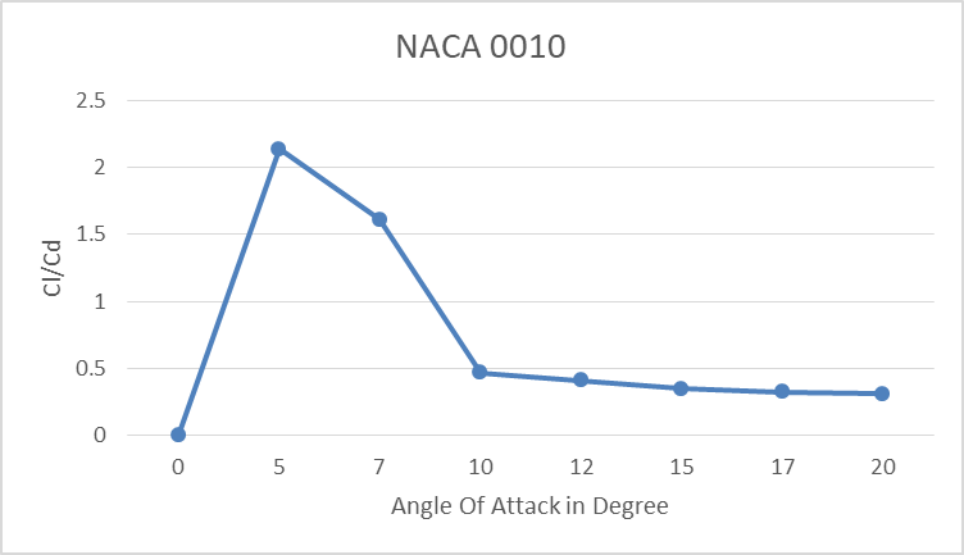

Fig 9.5: C_l/C_d vs AoA of NACA 0010 airfoil

From Fig 9.5, which shows the graph plotted between C_l/C_d and angle of attack, it is observed that the lift to drag ratio linearly varies with angle of attack and becomes constant when the flow over the airfoil just starts to get separated. The lift to drag ratio starts to decrease with angle of attack when the airfoil approaches the stalling condition.

9.2 Results of NACA 2410 Airfoil

After the Boundary conditions specified for the airfoil is initialized and the calculations are completed the following CFD results are available

Table 9.2: CFD results of NACA 2410 airfoil at velocity of 10m/s

AOA	C_l	C_d	C_l/C_d
0	0.0085	0.02246	0.378

5	0.06171	0.04202	1.468
7	0.09408	0.03359	2.801
10	0.10581	0.07125	1.485
12	0.07575	0.1636	0.463
15	0.0807	0.20033	0.403
17	0.08502	0.2216	0.384
20	0.09564	0.28575	0.335

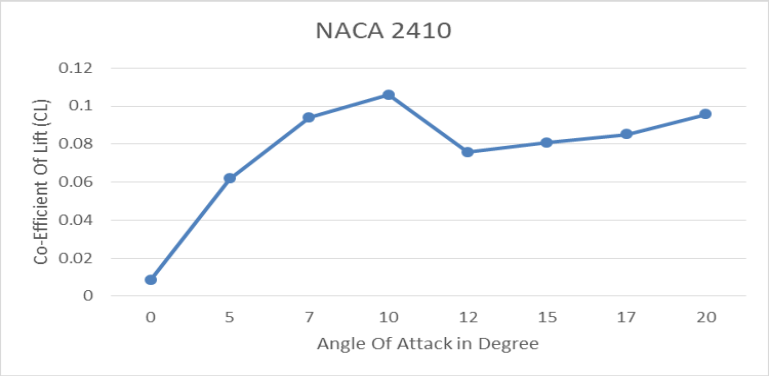

Fig 9.6: C*l* vs AoA of NACA 2410 Airfoil

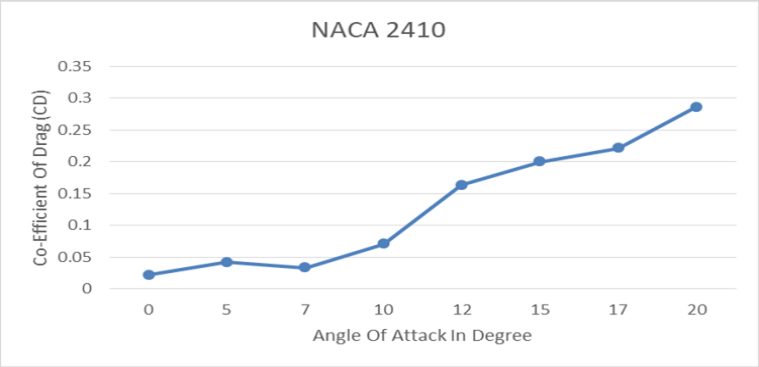

Fig 9.7: C*d* vs AoA of NACA 2410 Airfoil

From Fig 9.6 which shows the graph between C*l* and angle of attack and Fig 9.7 shows the graph between Cd and angle of attack, it is observed that cambered airfoil produces lift for zero angle of attack and produces higher lift than symmetrical airfoil at same angle of attack. Cambered airfoil has better lift distribution when compared to symmetrical airfoil.

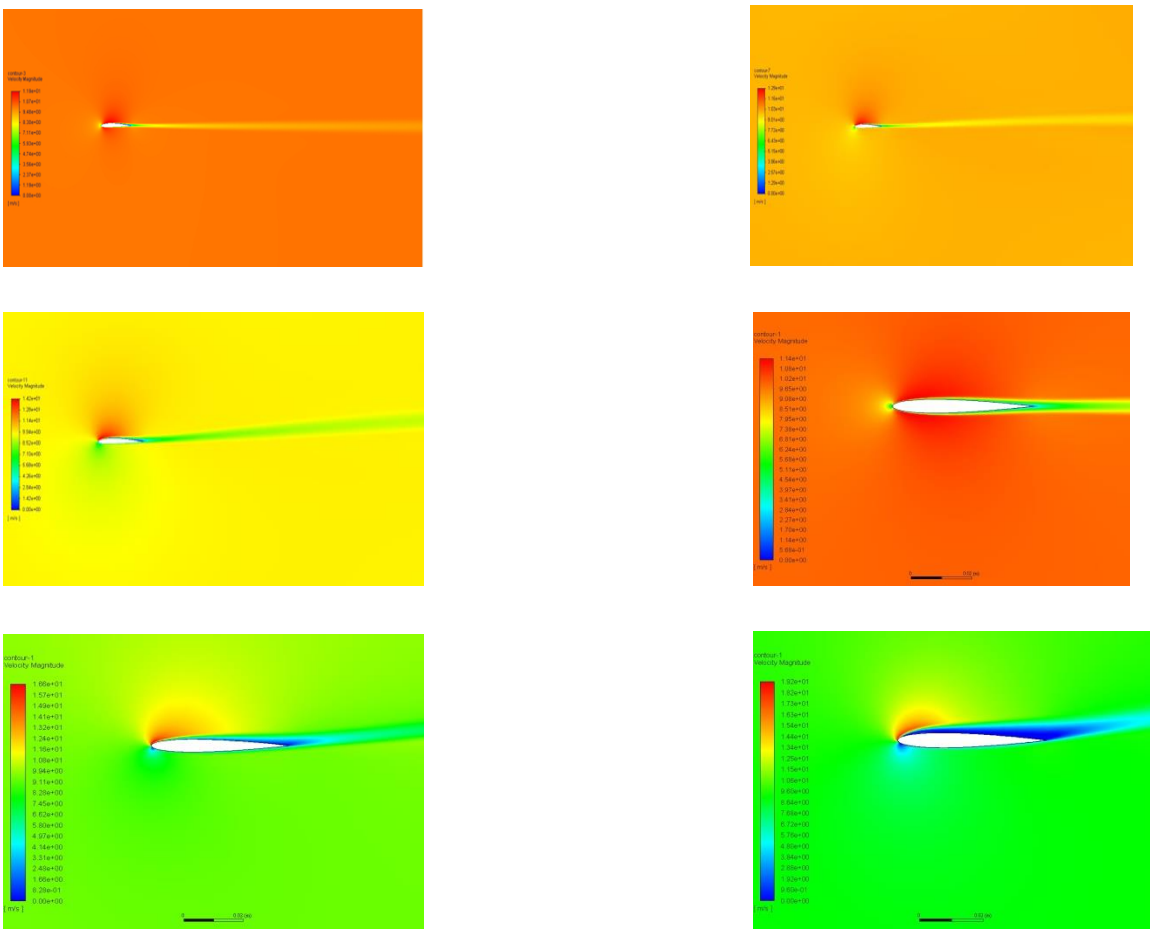

Fig 9.8: Velocity contours of NACA 2410 Airfoil at 0° (top left), 5° (top right), 7° (middle left), 10° (middle right), at stalling angle 15° (bottom left), 20° (bottom right)

From Fig 9.8, of velocity contours, it can be seen that the airfoil has equal velocity near both the upper and lower surface of the airfoil. The velocity above and below the airfoil is equal to the free stream velocity above the boundary layer of the airfoil. The velocity at the leading edge and trailing edge are slightly less when compared to the free stream velocity. The airflow gets obstructed by the leading surface of the airfoil, thus creating a stagnant point near the leading edge. As the angle of attack increases, the stagnant point starts moving towards the trailing edge. The flow over the upper surface of the airfoil gets separated from the boundary.

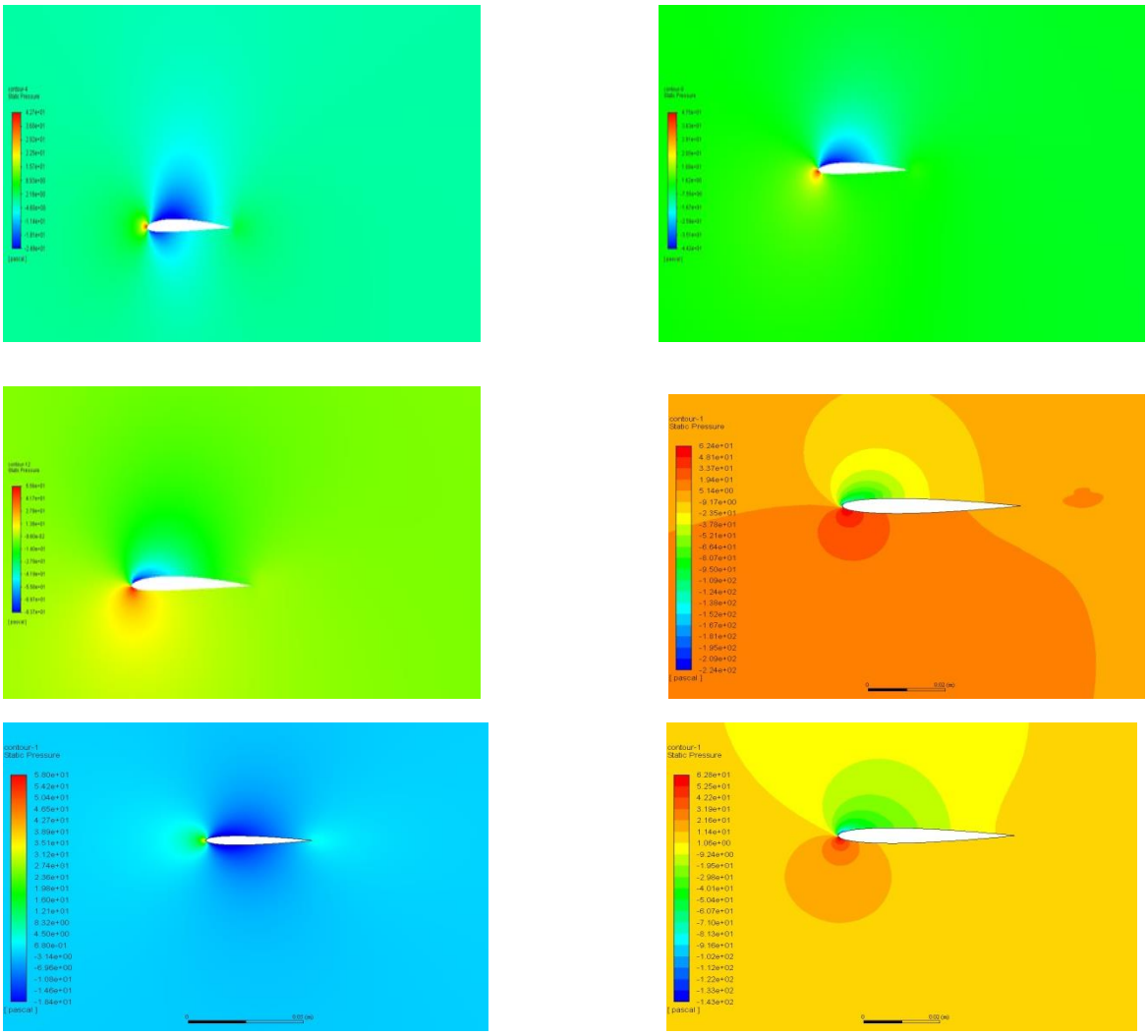

Fig 9.9: Pressure contours of NACA 2410 Airfoil at 0° (top left), 5° (top right), 7° (middle left), 10° (middle right), at stalling angle 15° (bottom left), and 20° (bottom right)

From Fig 9.9, of pressure contours of NACA 2410 Airfoil, it is deduced that the pressure distribution across the lower surface of the airfoil is higher even at zero angle of attack. Thus producing lift even at zero angle of attack. As the angle of attack increases the pressure distribution starts to curl over the upper surface of the airfoil. Due to the boundary layer separation across the upper surface of the airfoil, the curls start rotating more vigorously thus disturbing the flow.

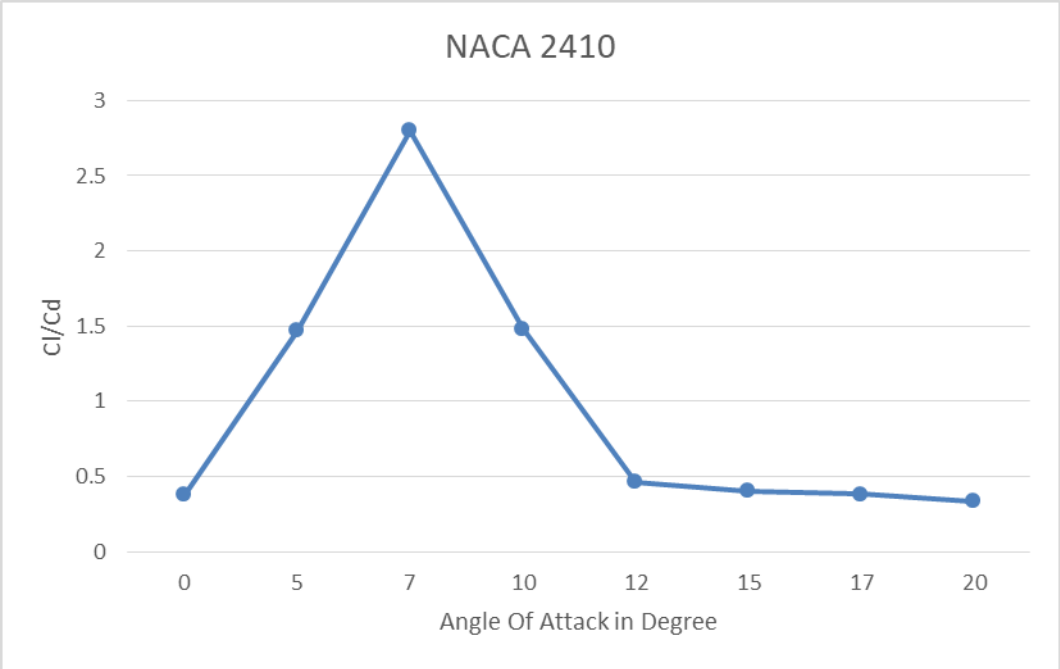

Fig 9.10: C*l* /C*d* vs AoA of NACA 2410 Airfoil

From Fig 9.10 which shows graph plotted between C*l*/Cd and AoA, it is observed that as the amount of lift increases, the amount of drag induced on the airfoil due to lift is also increased. This results in decrease in the aerodynamic performance of the airfoil.

9.3 Results of Corrugation Airfoil

After the Boundary conditions specified for the airfoil is initialized and the calculation are completed the following CFD results are available:

Table 9.3: CFD results of corrugated airfoil at velocity of 10m/s

AOA	C*l*	C*d*	C*l* /C*d*
0	0.004413	0.0069092	0.6387
5	0.024174	0.0075672	3.1945
7	0.030525	0.0080069	3.8123
10	0.037709	0.0091322	4.1292
12	0.040515	0.010036	4.0369
15	0.045236	0.012405	3.6465
17	0.046198	0.013131	3.1582
20	0.056641	0.019152	2.9574

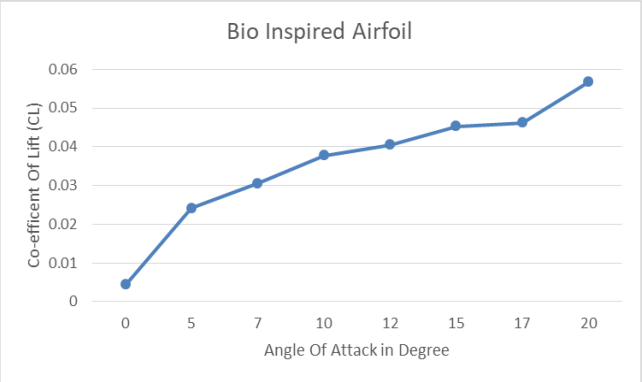

Fig 9.11: C*l* vs AoA of Corrugated Airfoil

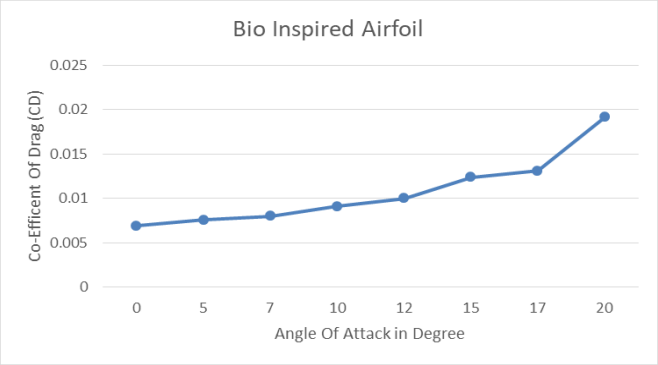

Fig 9.12: C*d* vs AoA of Corrugated Airfoil

From Fig 9.11 which shows the graph plotted between the coefficient of lift and angle of attack and Fig 9.12 which shows the graph plotted between the coefficient of drag and angle of attack, it seen that corrugated airfoil produces lift even at zero angle of attack. The airfoil stalls at an angle of 20°.

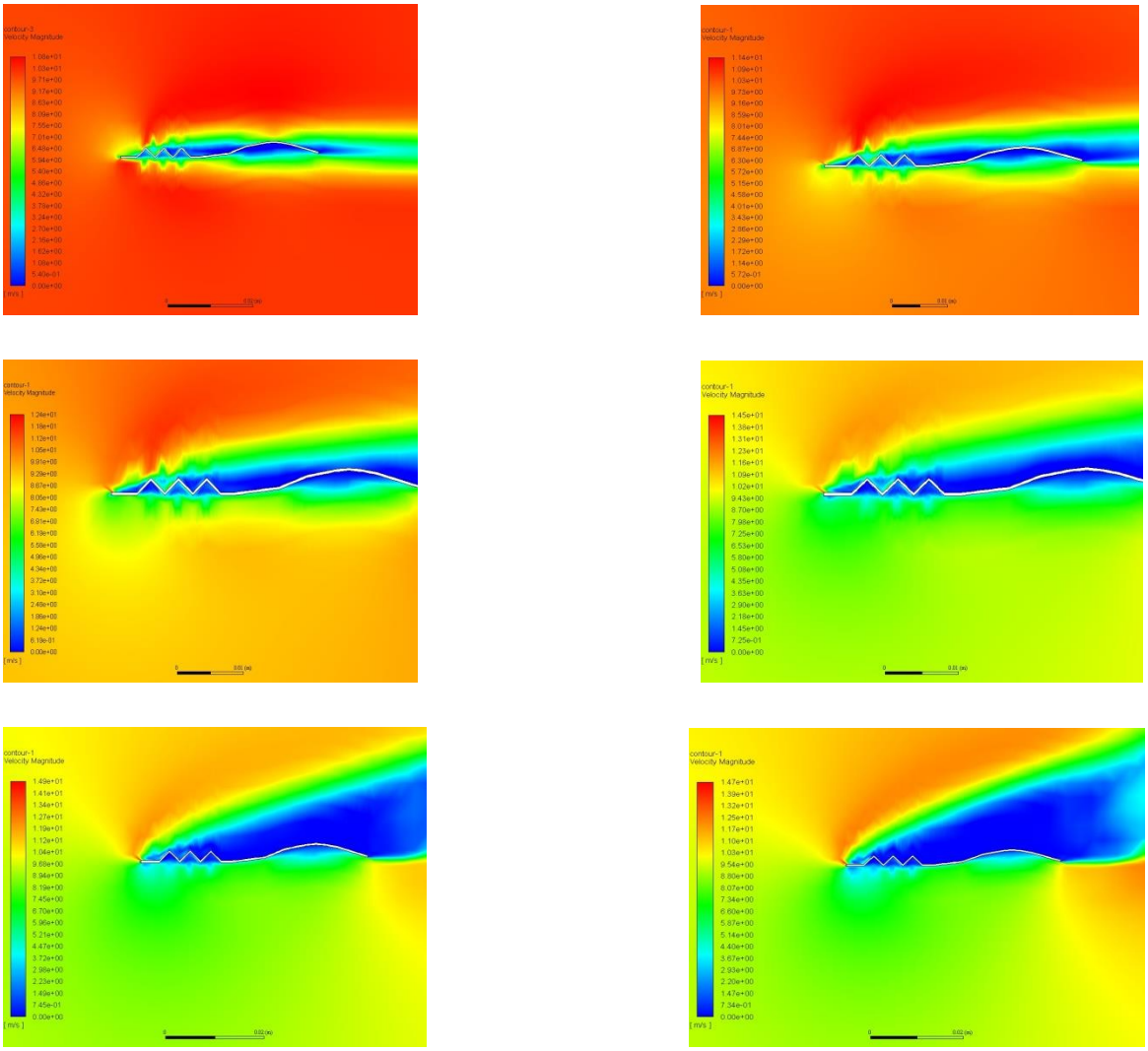

Fig 9.13: Velocity contours of corrugated airfoil at AOA of 0° (top left), 5° (top right), 7° (middle left), 10° (middle right), of 16° (bottom left), 20° (bottom right)

From Fig 9.13 of velocity contours of corrugated airfoil, it is observed that as the angle of attack increases the eddy currents or curls formed near the leading edge gets trapped inside the ridges. As a result the flow does not get disturbed. At higher angles of attack the curls start moving along the ridges and finally get separated and thus disturbing the flow causing boundary layer separation.

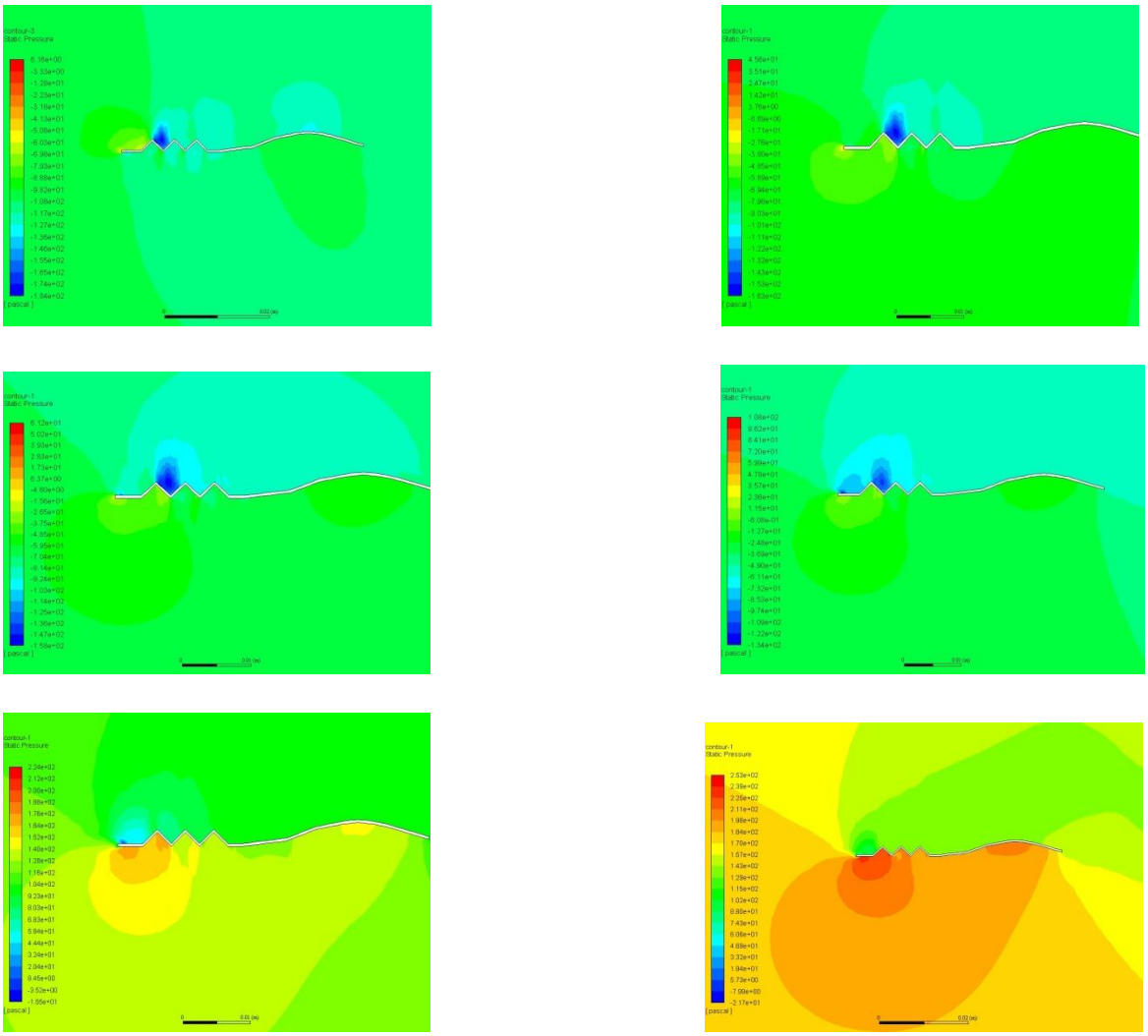

Fig 9.14: Pressure contours of corrugated airfoil at AOA of 0° (top left), 5° (top right), 7° (middle left), 10° (middle right), of 16° (bottom left), and 20° (bottom right)

From Fig 9.14 of pressure contours of corrugated airfoil, it is deduced that airfoil produces lift even at zero angle of attack. As observed during the zero degree angle of attack the pressure near the leading edge is higher than the lower surface of the airfoil. As the angle of attack increases, the pressure across the lower surface of the airfoil seems to be higher. And the curls which get trapped inside the ridges do not affect the flow. As the airfoil approaches stall, the curls starts to disrupt the flow causing boundary layer separation.

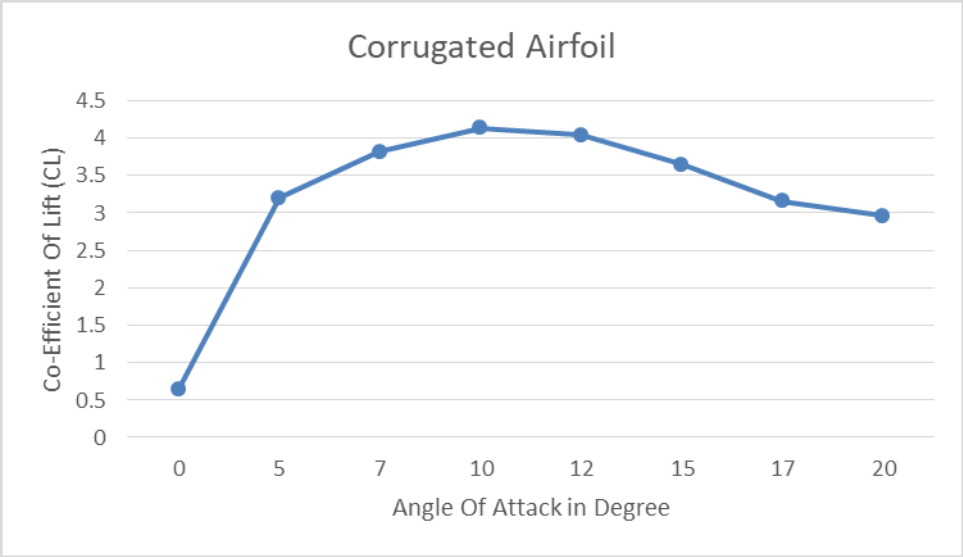

Fig 9.14: C_l/C_d vs AoA of corrugated airfoil

From Fig 9.14 which shows a graph plotted between the lift to drag ratio and angle of attack, it is observed that corrugated airfoil has higher performance at higher angle of attack. The lift and drag produced compensates each other quality.

9.4 Comparison of Corrugated Airfoil with Conventional Airfoil

Table 9.4: Table Comparison of C_l/C_d

AOA (Degrees)	C_l/C_d (NACA 0010)	C_l/C_d (NACA 2410)	C_l/C_d (Conventional Airfoil)
0°	0	0.3785	0.5978
5°	2.14	1.4685	3.1946
7°	1.612	2.8008	3.8124
10°	0.4703	1.485	4.1292
12°	0.4092	0.463	4.037
15°	0.3508	0.4028	3.6466
17°	0.3264	0.3836	3.5182
20°	0.0312	0.3326	2.8505

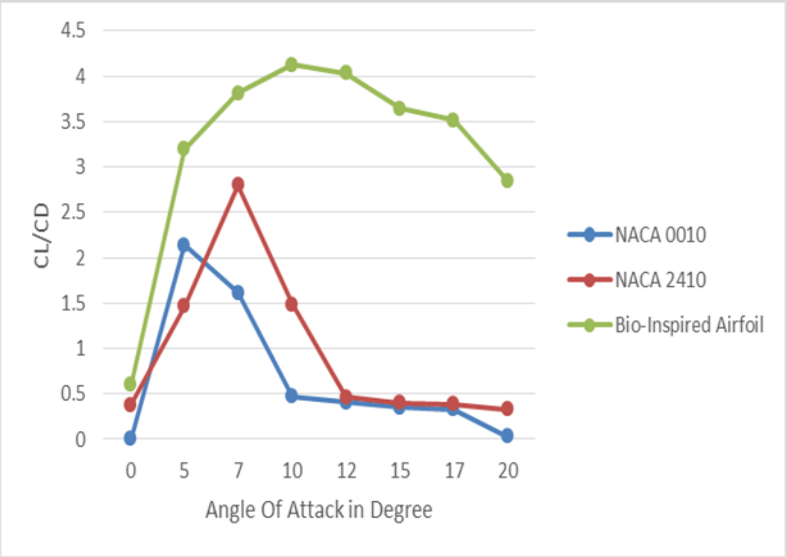

Fig 9.15: AoA vs Cl/Cd

Table 9.5: Comparison of Cl/Cdmax of corrugated airfoil with conventional airfoils

Airfoil	Cl/Cdmax
Corrugated Airfoil	2.140
NACA 0010	2.8008
NACA 2410	4.1292

From observing the velocity contours of the corrugated airfoil and conventional airfoil, the effect of flow air separation on the aerodynamic flow can be easily determined. For conventional airfoils such as the NACA 2410 airfoils, the incoming fluid streams flow smoothly along the streamlined nose and the flow separation takes place near the trailing edge of the airfoil.

For corrugated airfoil, the bubble vortex formation formed near the leading edge gets trapped in the ridges as the angle of attack increases. Thus delaying the boundary layer separation and also helps in reattachment of the flow over the curved streamlined trailing edge of the airfoil.

From observing the above comparison graph of Cl/Cd of corrugated airfoil and other conventional airfoils, the corrugated airfoil proves to be producing higher lift-of-drag ratio than other conventional airfoil such as NACA 0010 and NACA 2410 and also the corrugated airfoil has a higher stalling angle compared to other conventional airfoils.

Table 9.6: Percentage Increase in Cl/Cd

Cl/Cd (Conventional airfoil)	Cl/Cd (Corrugated airfoil)	Percentage Increase in Cl/Cd
2.8008 (NACA 0010)	2.140	
4.1292 (NACA 2410)		

CHAPTER- 10

CONCLUSION AND FUTURE SCOPE

10.1 CONCLUSION

In this project, to explore the potential applications of MAV's and to overcome the limitations of the conventional airfoils at low Reynolds number, the use of corrugated airfoil is proposed. The design of the Corrugated airfoil was inspired through the wing structure of the dragonfly. The corrugations provoke an early transition to turbulent flow over the two-dimensional airfoil permitting reattachment of the flow.

The shape of the corrugations plays a key role in generating vortices. The vortices which are formed near the leading edges get trapped in the ridges of the corrugated airfoil. A fluid roller bearing effect is created over the virtual airfoil when the trapped vortices merge with other; the travelling wave produced by the virtual boundary around the fluid roller bearings avoids the formation of boundary layer on the virtual surface, thereby leading to high aerodynamic performance.

It is found that the lift co-efficient increase as the number of vortices increases o the suction surface, also it is shown that the partially merged co-rotating vortices give higher lift as compared to fully merged vortices. As the angle of attack increase, airflow would separate from the leading edge to form a separation bubble, and the separated flow would reattach sooner due to the corrugation compared with smooth airfoils.

From the comparative results between Corrugated Airfoil and Conventional Airfoils, we can see that the Corruagted airfoil has much higher C*l*/Cdmax of and stalling at an angle of 20 degrees. When compared to NACA 0010 which has a C*l*/Cdmax of and stalls at an angle of 16 degrees. And also, the NACA 2410 airfoil has a C*l*/Cdmax of and stalls at an angle of 20 degrees.

From observing the table of percentage increase in C*l*/Cdmax, there is an increase of about 8.7% and 4.67% in C*l*/Cdmax of corrugated airfoil when compared to NACA 0010 and NACA 2410 airfoils respectively.

Thus, the performance characteristics that determines the airworthiness of an airfoil i.e., **Cl**/Cdmax is higher for corrugated airfoil. Hence it is best suited airfoil for MAV's flying at low Reynolds Number.

10.2 FUTURE SCOPE

- Computational analysis for different number of corrugations, shape and angle of corrugations.
- Fabrication and Wind tunnel testing of corrugated wing for experimental validation.
- Shape Optimization of corrugated airfoil.

CHAPTER-11

REFERENCES

[1] Tamai, Wang, Hai Hu " Aerodynamic Performance of a corrugated DragonflyAir foil Compared with Smooth Air foils at Low Reynolds Number" 45th AIAA Aerospace sciences meeting and exhibit 8-11 January 2007.

[2] Kesel, A. B., Philippi, U. and Nachtigall, W., "Biomechanical Aspects of Insect Wings – An Analysis using the Finite Element Method," Computers in Biology And Medicine, Vol. 28, 1998, pp. 423–437.

[3] Shridhar V K, Dwivwdi Y D, "Effect of Peak Shape in Bio Inspired Corrugated Wing" SSRN Electronic Journal -January 2017.

[4] T H New, Chung Hoang, Shi, "Effects of Corrugated aerofoil Surface Features on Flow- Separation Control" AIAA Journal- January 2014.

[5] Carmichael, B. H., 1981, "Low Reynolds number aerofoil Survey", Vol. 1, NASA CR-165803, 1981.

[6] P Pradeep Kannah, G Balaji, S Arunvinthan, "AerodynamicCharacteristics of Dragonfly Wing Section" IJIRRSET-Vol.5, Special Issue 8-May 2016.

[7Xue Gaung Meng, Lei Xu , Mao sun "Aerodynamic effects of Corrugation in Flapping Insect Wings in Hovering Flight" The Journal of Experimental Biology 214,432-444-October 2010.

[8] Wei Hua Ho, T H New "CFD Analysis of Bio-inspired Corrugated aerofoils" 11th International Conference of Fluid Dynamics-December 2013.

[9] Levy DE, Seifert A (2009),"Simplified dragonfly aerofoil aerodynamics at Reynolds Numbers below 8000", Physics Fluids 21(7):071,901.

[10]Thomos J Mueller "On the Birth of Micro Air Vet" Volumelume 1-January 2019

[11]Maria Mingallon, Sakthivel Ramaswamy " The Architecture of the Dragonfly Wing: A Study of the Structural and Fluid Dynamic Capabilities of the Anisoptera's Forewing" IMECE2011-November 2011, Denver, Colorado, USA

[12] Stefen Jongerius, D Lentink "Structural Analysis of a Dragonfly Wing" Experimental Mechanics 50"1323-1334-November 2010

[13] Dilek Funda Kurutulus " Introduction to Micro Air Vehicles: Design, Concepts and Applications" Chapter 5-April 2011

APPENDIX

Co-ordinates of corrugated aerofoil, chord length=55mm, thickness=0.5mm

Sl.no	x-coordinates	y-coordinates
1	0	0
2	4.5	0
3	7	2.5
4	9.5	0
5	12	2.5
6	14.5	0
7	17	2.5
8	19.5	0
9	22	0
10	30	1
11	35	3
12	40	4
13	42.5	4.25
14	45	4
15	47.5	3.5
16	50	2.75
17	52.5	2
18	55	1.25